Earth and Planetary Science Letters 449 (2016) 228–239

Contents lists available at ScienceDirect

Earth and Planetary Science Letters

www.elsevier.com/locate/epsl

Groundwater storage changes in the Tibetan Plateau and adjacent areas revealed from GRACE satellite gravity data

Longwei Xiang [a,b], Hansheng Wang [a,*], Holger Steffen [c], Patrick Wu [d], Lulu Jia [e], Liming Jiang [a], Qiang Shen [a]

[a] State Key Laboratory of Geodesy and Earth's Dynamics, Institute of Geodesy and Geophysics, Chinese Academy of Sciences, Wuhan 430077, China
[b] University of Chinese Academy of Sciences, Beijing 100049, China
[c] Lantmäteriet, 80182 Gävle, Sweden
[d] Department of Earth Sciences, University of Hong Kong, Hong Kong
[e] National Earthquake Infrastructure Service, Beijing 100036, China

ARTICLE INFO

Article history:
Received 27 October 2015
Received in revised form 2 June 2016
Accepted 3 June 2016
Available online 15 June 2016
Editor: P. Shearer

Keywords:
satellite gravity
GRACE
groundwater storage
Tibetan Plateau and surroundings
river basins

ABSTRACT

Understanding groundwater storage (GWS) changes is vital to the utilization and control of water resources in the Tibetan Plateau. However, well level observations are rare in this big area, and reliable hydrology models including GWS are not available. We use hydro-geodesy to quantitate GWS changes in the Tibetan Plateau and surroundings from 2003 to 2009 using a combined analysis of satellite gravity and satellite altimetry data, hydrology models as well as a model of glacial isostatic adjustment (GIA). Release-5 GRACE gravity data are jointly used in a mascon fitting method to estimate the terrestrial water storage (TWS) changes during the period, from which the hydrology contributions and the GIA effects are effectively deducted to give the estimates of GWS changes for 12 selected regions of interest. The hydrology contributions are carefully calculated from glaciers and lakes by ICESat-1 satellite altimetry data, permafrost degradation by an Active-Layer Depth (ALD) model, soil moisture and snow water equivalent by multiple hydrology models, and the GIA effects are calculated with the new ICE-6G_C (VM5a) model. Taking into account the measurement errors and the variability of the models, the uncertainties are rigorously estimated for the TWS changes, the hydrology contributions (including GWS changes) and the GIA effect. For the first time, we show explicitly separated GWS changes in the Tibetan Plateau and adjacent areas except for those to the south of the Himalayas. We find increasing trend rates for eight basins: $+2.46 \pm 2.24$ Gt/yr for the Jinsha River basin, $+1.77 \pm 2.09$ Gt/yr for the Nujiang-Lancangjiang Rivers Source Region, $+1.86 \pm 1.69$ Gt/yr for the Yangtze River Source Region, $+1.14 \pm 1.39$ Gt/yr for the Yellow River Source Region, $+1.52 \pm 0.95$ Gt/yr for the Qaidam basin, $+1.66 \pm 1.52$ Gt/yr for the central Qiangtang Nature Reserve, $+5.37 \pm 2.17$ Gt/yr for the Upper Indus basin and $+2.77 \pm 0.99$ Gt/yr for the Aksu River basin. All these increasing trends are most likely caused by increased runoff recharges from melt water and/or precipitation in the surroundings. We also find that the administrative actions such as the Chinese Ecological Protection and Construction Project help to store more groundwater in the Three Rivers Source Region, and suggest that seepages from the Endorheic basin to the west of it are a possible source for GWS increase in this region. In addition, our estimates for GWS changes basically confirm previous results along Afghanistan, Pakistan, north India and Bangladesh, and clearly reflect the excessive use of groundwater. Our results will benefit the water resource management in the study area, and are of particular significance for the ecological restoration in the Tibetan Plateau.

1. Introduction

The Tibetan Plateau is characterized by its high altitude and extensive size. Water storage variation and ecosystem reserve receive increased attention as groundwater storage (GWS) is critical for grazing, breeding, farming, manufacturing and ecosystem restoring in the plateau. Knowledge of GWS changes is also important for geologic disaster prevention and control, engineering design (e.g., for dams, tunnels, mines and slopes) and geothermal exploitation. In addition, groundwater recharges several distinct rivers in India, Bangladesh, China and Southeast Asia, promoting regional economy and social development. Major rivers include the Indus

* Corresponding author.
E-mail address: whs@asch.whigg.ac.cn (H. Wang).

http://dx.doi.org/10.1016/j.epsl.2016.06.002

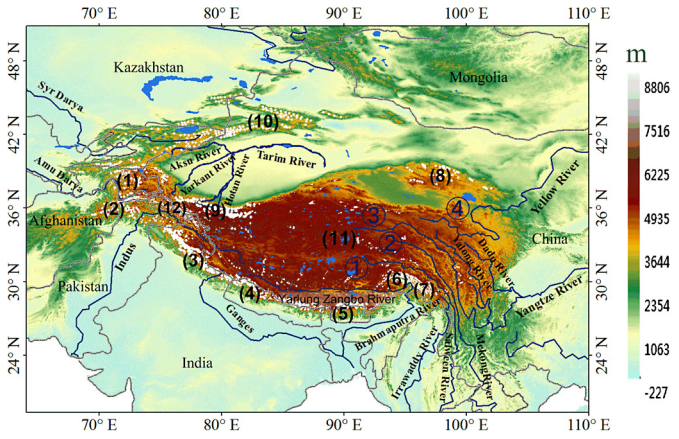

Fig. 1. Map of the Tibetan Plateau and adjacent areas with topography based on Shuttle Radar Topography Mission (SRTM) digital elevation data (Jarvis et al., 2008). The 957 white dots denote the equivalent point masses of glacier mass budgets observed by ICESat-1 (Gardner et al., 2013). Numbers in brackets denote the glacier sub-regions: (1) Hissar Alay and Pamir, (2) Hindu Kush, (3) West Himalaya, (4) Center Himalaya, (5) East Himalaya, (6) South and East Tibet, (7) Hengduan Shan, (8) Qilian Shan, (9) West Kunlun, (10) Tien Shan, (11) East Kunlun and Inner Tibet and (12) Karakoram. Lakes and rivers are in blue. Rivers in the source regions of the eastern plateau: ① Nujiang River, ② Lancangjiang River, ③ Yangtze River, ④ Yellow River. ②, ③ and ④ together is usually called as the Three Rivers.

River, Brahmaputra River, Yarlung Zangbo River, Yangtze River, Yellow River, Irrawaddy River, Salween River and Mekong River. Last but not least, understanding the groundwater changes also plays an important role for the development of hydrology models which allow reliable projections for water resource management and thus guaranteeing the sustainability of economic and societal growth.

However, unlike glaciers/snow-caps, groundwater is basically invisible and its contribution to water resource, the hydrologic cycles and the response to increased warming are rarely known. Since the plateau is far inland with harsh weather conditions and challenging geography, only a few well water level observations for GWS changes were made, and hydrology and weather stations are sparsely distributed. In this case, the hydrology models available (e.g., WaterGAP Global Hydrology Model, WGHM, Döll et al., 2003) have difficulties explaining the GWS changes in the area. Our aim is to provide insight into GWS changes of the Tibetan Plateau. Due to signal leakage of gravity data used, adjacent areas are included in our investigation as well (Fig. 1).

In the plateau, the groundwater is controlled by permafrost, topography, geomorphology, tectonics and surface hydrology. Permafrost is usually used as a reference for its classification. In the sense of the storage position with respect to permafrost, the groundwater is classified as supra-permafrost water, in-permafrost water and sub-permafrost water (Cheng and Jin, 2013). The near-surface shallow groundwater above the permafrost base is most sensitive to seasonal climatic changes (Ge et al., 2008).

The groundwater flow in the plateau is usually driven and sustained by the topographic gradient and recharge at high elevations (Ge et al., 2008) by precipitation, snow- and ice-melt water, and is discharged in basins and valleys (Cheng and Jin, 2013). Groundwater circulation can reach more than 1 to 2 km in depth (Ge et al., 2008). In the Endorheic basin (most parts between 80°E and 92°E in the Tibetan Plateau), Zhou et al. (2013) found a large water loss in the Lake Nam Co (30.5°N, 90.6°E) due to water seepage. Chen and Wang (2012) inferred that the seepage water in the Endorheic basin could be transported by deep hydrological cycles along some suture zones to the eastern Plateau. Accordingly, in the Tibetan Plateau the groundwater may have a very special storage at depth, and the groundwater cycles could reach very deep aquifers and could stretch out over large distances.

In order to better evaluate the GWS changes, we turn to hydrogeodesy and remove known contributions (soil moisture, glacier ice melting etc.) from terrestrial water storage (TWS) changes observed by the Gravity Recovery and Climate Experiment (GRACE) mission (Bettadpur, 2012). So far, most works in the Tibetan Plateau are focused on monitoring TWS changes (e.g., Zhong et al., 2009; Haile, 2011), or glacier ice melting (e.g., Matsuo and Heki, 2010; Jacob et al., 2012; Yi and Sun, 2014). Although Jin and Feng (2013) estimated the global GWS changes with GRACE gravity data together with hydrological models GLDAS (Global Land Data Assimilation System) (Rodell et al., 2004) and WGHM (Döll et al., 2003), the glacier ice melting and lake water changes were not precisely removed from TWS changes. Similarly, GWS changes were also estimated with GRACE gravity data and hydrology models by many studies for the investigation of groundwater depletion in northern India. However, these results could be affected by gravity signal leakage from ice melting in the Himalayas. Most works did not try to exclude the leakage effects (e.g., Matsuo and Heki, 2010). Although Rodell et al. (2009) evaluated and removed the leakage effects, the mountain glaciers considered only have 6% of the total mountain range length, and the ice melt rate was assumed to be the same as that for the entire Himalayas glaciers during 1962–2004 (not matching the surveyed period). This may cause additional errors in the estimates of GWS changes for this area. J.L. Chen et al. (2014) followed Rodell et al. (2009) in removing the leakage effects. Yi and Sun (2014) and Tiwari et al. (2009) suppressed the leakage effects from neighboring glaciers with an inversion method. In addition, glacial isostatic adjustment (GIA) due to melting of ice sheets in the far field may induce mantle flow and surface mass redistribution around the Earth (Peltier et al., 2015). Such effects should be carefully estimated with improved GIA model and removed from GRACE observations.

Recently, improvements have been made in our study area for monitoring glacier melting, lake water level and permafrost degradation, which allows a better separation of the GWS changes from the GRACE-derived TWS changes. Most glaciers in the Himalayas and Tien Shan are found to have undergone melting from 2003 to 2009 according to the analyses of Ice, Cloud, and land Elevation Satellite (ICESat-1) elevation data and the digital elevation model from the Shuttle Radar Topography Mission (SRTM) (Kääb et al., 2012, 2014; Gardner et al., 2013). Yao et al. (2012) investigated the changes in glaciers status with topographic maps, satellite images and in-situ observation. Water levels for most lakes in the plateau are found to rise over the same period mainly based on ICESat-1 data (Zhang et al., 2011, 2013) while they were decreasing for most lakes northwest to the Tien Shan based on in-situ measurements (Farinotti et al., 2015). In the Tibetan Plateau, long-term trend of Active-Layer Depth (ALD, defined as the depth of the layer which freezes and thaws every year) thickening were simulated by Oelke and Zhang (2007), which can be used to estimate the resultant hydrology contributions.

This study focuses on the separation of 7 years of GWS changes in the Tibetan Plateau and its surroundings (Fig. 1, east longitudes between 65° and 110° and north latitudes between 20° and 50°). Multiple new data and models are incorporated: Release-5 GRACE gravity data (Bettadpur, 2012), glacier mass budget data (Gardner et al., 2013), lake water level data (Zhang et al., 2011), an ALD model (Oelke and Zhang, 2007), and a new GIA model (Argus et al., 2014; Peltier et al., 2015). The surveyed period in this study ranges from January 2003 to December 2009, thus matching to a large degree the time span of the ICESat-1 mission.

In the next section, the methodology is introduced, followed by a description and discussion of the results in sections 3 and 4. Finally, the conclusions are summarized in section 5. The data used

and the processing techniques involved are stated in the section A of Supplementary material.

2. Methodology

The terrestrial water storage (TWS) basically consists of soil moisture (SM), glacier ice (ICE), snow water equivalent (SWE), lake water (LAKE), permafrost (PM) and groundwater storage (GWS) in our study area. To quantify the GWS changes in the area, the changes of 5 hydrology components from hydrology models or measurements and the GIA effects must be effectively removed from TWS changes observed by GRACE. In this section, we present the spherical harmonic (SH) expressions of the changes of TWS and the components at sites, show the formulas for mascon fitting inversion and derive the formulas for error variances. The methodology showed here is also valid for estimating the trend of GWS changes during the surveyed period.

2.1. SH expressions of the TWS change and the hydrology contributions as well as the GIA effect

At any arbitrary site with co-latitude θ and longitude ϕ in our study area, the TWS change between any two times (in equivalent water thickness, EWT) can be expressed by a sum of spherical harmonics (Wahr et al., 1998),

$$\Delta T^{\mathrm{TWS}}(\theta,\phi)=\sum_{l=0}^{\infty}\sum_{m=0}^{l}\left(\Delta c_{lm}^{\mathrm{TWS}}\cos m\phi+\Delta s_{lm}^{\mathrm{TWS}}\sin m\phi\right)\times\tilde{P}_{lm}(\cos\theta), \tag{1}$$

$$=\frac{a\rho_{ave}}{3\rho_w}\sum_{l=0}^{\infty}\sum_{m=0}^{l}\frac{2l+1}{1+k_l}\times(\delta c_{lm}\cos m\phi+\delta s_{lm}\sin m\phi)\tilde{P}_{lm}(\cos\theta), \tag{2}$$

in which $\Delta c_{lm}^{\mathrm{TWS}}$ and $\Delta s_{lm}^{\mathrm{TWS}}$ are the spherical harmonic (SH) coefficients, δc_{lm} and δs_{lm} are the changes in Stokes coefficients from monthly GRACE data, $\tilde{P}_{lm}(\cos\theta)$ is the lth degree and mth order normalized associated Legendre polynomial, k_l is the degree l elastic load Love number of the Preliminary Reference Earth Model for potential perturbation (Wang et al., 2012), ρ_{ave} is the average density of the earth (5.517 g/cm^3), ρ_w is the water density (1 g/cm^3) and a is the radius of the Earth.

The change (in EWT) for the hydrology component K (= SM, ICE, SWE, LAKE or PM) can be represented as

$$\Delta T^{K}(\theta,\phi)=\sum_{l=0}^{\infty}\sum_{m=0}^{l}\left(\Delta c_{lm}^{K}\cos m\phi+\Delta s_{lm}^{K}\sin m\phi\right)\tilde{P}_{lm}(\cos\theta), \tag{3}$$

where the SH coefficients Δc_{lm}^{K} and Δs_{lm}^{K} can be given with SH analysis of the 'observed' changes ΔW^K (in EWT, from models or observations) for the selected component in our surveyed area (Ω),

$$\begin{cases}\Delta c_{lm}^{K}=\dfrac{1}{4\pi}\displaystyle\int_{\Omega}\Delta W^{K}(\theta',\phi')\tilde{P}_{lm}(\cos\theta')\cos m\phi' d\Omega'\\ \Delta s_{lm}^{K}=\dfrac{1}{4\pi}\displaystyle\int_{\Omega}\Delta W^{K}(\theta',\phi')\tilde{P}_{lm}(\cos\theta')\sin m\phi' d\Omega'\end{cases}, \tag{4}$$

with $d\Omega'=\sin\theta' d\theta' d\phi'$.

If ΔW^K within Ω can be discretized as point mass assemble ΔM_j^K at (θ_j',ϕ_j') $(j=1,2,\ldots,N^K)$, the discretized expression of Eq. (4) is then given as,

$$\begin{cases}\Delta c_{lm}^{K}=\displaystyle\sum_{j=1}^{N^K}\frac{\Delta M_j^K}{4\pi a^2\rho_w}\tilde{P}_{lm}(\cos\theta_j'^{K})\cos m\phi_j'^{K}\\ \Delta s_{lm}^{K}=\displaystyle\sum_{j=1}^{N^K}\frac{\Delta M_j^K}{4\pi a^2\rho_w}\tilde{P}_{lm}(\cos\theta_j'^{K})\sin m\phi_j'^{K}\end{cases}. \tag{5}$$

The GIA effect (in EWT, given by a GIA model) on TWS change at a site can be also expressed by Eq. (1) and calculated by Eq. (2) for $K=$ GIA. ΔW^K ($K=$ GIA) are given by synthesis using Eq. (1) and can also be used in Eq. (4) to get the discretized point mass assemble (DPMA).

It will be seen that the DPMA, based on the 'observed' ΔW^K for ICE, LAKE, PM and GIA in this study, is useful in the estimation of error variances.

The GWS change at the observed site over two times can be computed by

$$\Delta T^{\mathrm{GWS}}(\theta,\phi)=\sum_{l=0}^{\infty}\sum_{m=0}^{l}\left(\Delta c_{lm}^{\mathrm{GWS}}\cos m\phi+\Delta s_{lm}^{GWS}\sin m\phi\right)\times\tilde{P}_{lm}(\cos\theta), \tag{6}$$

with the separated SH coefficients

$$\begin{pmatrix}\Delta c_{lm}^{\mathrm{GWS}}\\ \Delta s_{lm}^{\mathrm{GWS}}\end{pmatrix}=\begin{pmatrix}\Delta c_{lm}^{\mathrm{TWS}}\\ \Delta s_{lm}^{\mathrm{TWS}}\end{pmatrix}-\begin{pmatrix}\Delta c_{lm}^{\mathrm{SM}}\\ \Delta s_{lm}^{\mathrm{SM}}\end{pmatrix}-\begin{pmatrix}\Delta c_{lm}^{\mathrm{ICE}}\\ \Delta s_{lm}^{\mathrm{ICE}}\end{pmatrix}-\begin{pmatrix}\Delta c_{lm}^{\mathrm{SWE}}\\ \Delta s_{lm}^{\mathrm{SWE}}\end{pmatrix}-\begin{pmatrix}\Delta c_{lm}^{\mathrm{LAKE}}\\ \Delta s_{lm}^{\mathrm{LAKE}}\end{pmatrix}-\begin{pmatrix}\Delta c_{lm}^{\mathrm{PM}}\\ \Delta s_{lm}^{\mathrm{PM}}\end{pmatrix}-\begin{pmatrix}\Delta c_{lm}^{\mathrm{GIA}}\\ \Delta s_{lm}^{\mathrm{GIA}}\end{pmatrix}. \tag{7}$$

As seen above, the change of TWS and the hydrology components as well as the GIA effect at any site over two times can be computed with the SH expressions. They are labeled by 'SH' for convenience, e.g., SH TWS change.

2.2. Mascon-fitting formulas

If the SH GWS changes are simply used to estimate the total GWS change for a region of interest, the results are inevitably affected by signal leakages due to the truncation of higher harmonic degree terms and necessary filtering (e.g, using Gaussian filter, Jekeli, 1981). The way used here is the mascon fitting treatment (Jacob et al., 2012), which can avoid the problem to a large degree. In the following, we follow Jacob et al. (2012) to outline the basic formulas for GWS changes and the budgets at mascons, and we also derive the expressions of related error variances.

In our study area, we can define M independent mascons (see Section 2.3.2), based on the anomalies of SH GWS changes. For each mascon, the GWS change over two times is assumed to be uniformly distributed with the EWT change of $\Delta T_i'^{\mathrm{GWS}}$ $(i=1,2,\ldots,M)$. SH analysis with Eqs. (3) and (4) is done respectively for each mascon with a uniformly distributed unit EWT (except that Ω now represents the mascon region considered), to generate the mascon SH coefficients $\Delta c_{lm}'^{i}$ and $\Delta s_{lm}'^{i}$ $(i=1,2,\ldots,M)$.

Then, minimizing the least-squares objective function,

$$E=\sum_{l=0}^{\infty}w_l^2\sum_{m=0}^{l}\left\{\left[\Delta c_{lm}^{\mathrm{GWS}}-\sum_{i=1}^{M}\Delta T_i'^{\mathrm{GWS}}\Delta c_{lm}'^{i}\right]^2+\left[\Delta s_{lm}^{\mathrm{GWS}}-\sum_{i=1}^{M}\Delta T_i'^{\mathrm{GWS}}\Delta s_{lm}'^{i}\right]^2\right\}, \tag{8}$$

to find $\Delta T_i'^{\mathrm{GWS}}$ $(i=1,2,\ldots,M)$ with

$$\Delta T_i'^{\mathrm{GWS}} = \sum_{j=1}^{M} A_{i,j}^{-1} \sum_{l=0}^{\infty} \sum_{m=0}^{l} w_l^2 \left(\Delta c_{lm}^{\mathrm{GWS}} \Delta c_{lm}'^{j} + \Delta s_{lm}^{\mathrm{GWS}} \Delta s_{lm}'^{j} \right), \quad (9)$$

in which w_l is the degree coefficient of Jekeli's Gaussian averaging function for Legendre expansion (Jekeli, 1981), $A_{i,j}^{-1}$ is the element of inverse of matrix A while elements of A are given by

$$A_{ij} = \sum_{l=0}^{\infty} \sum_{m=0}^{l} w_l^2 \left(\Delta c_{lm}'^{j} \Delta c_{lm}'^{i} + \Delta s_{lm}'^{j} \Delta s_{lm}'^{i} \right), \quad (10)$$

or,

$$\Delta T_i'^{\mathrm{GWS}} = \Delta T_i'^{\mathrm{TWS}} - \Delta T_i'^{\mathrm{SM}} - \Delta T_i'^{\mathrm{ICE}} - \Delta T_i'^{\mathrm{SWE}} - \Delta T_i'^{\mathrm{PM}} - \Delta T_i'^{\mathrm{GIA}}, \quad (11)$$

where the quantities on the right side are the changes of TWS and the components (in EWT) at the ith mascon, and can be also computed by Eq. (9) but using respective SH coefficients.

Assuming that the relevant errors are independent for the estimates of changes of TWS and the components at the mascon, the error variance for the estimate of GWS change at the ith mascon can be calculated by

$$\sigma^2_{\Delta T_i'^{\mathrm{GWS}}} = \sigma^2_{\Delta T_i'^{\mathrm{TWS}}} + \sigma^2_{\Delta T_i'^{\mathrm{SM}}} + \sigma^2_{\Delta T_i'^{\mathrm{ICE}}} + \sigma^2_{\Delta T_i'^{\mathrm{SWE}}} + \sigma^2_{\Delta T_i'^{\mathrm{LAKE}}} + \sigma^2_{\Delta T_i'^{\mathrm{PM}}} + \sigma^2_{\Delta T_i'^{\mathrm{GIA}}}. \quad (12)$$

Using Eqs. (9) and (5), we deduce the error variance for the estimate of K change ($K \neq$TWS)

$$\sigma^2_{\Delta T_i'^{K}} = \sum_{j'=1}^{N^K} \left[\sum_{l=0}^{\infty} \sum_{m=0}^{l} \left(\frac{\partial \Delta T_i'^{K}}{\partial \Delta c_{lm}^{K}} \frac{\partial \Delta c_{lm}^{K}}{\partial M_{j'}^{K}} + \frac{\partial \Delta T_i'^{K}}{\partial \Delta s_{lm}^{K}} \frac{\partial \Delta s_{lm}^{K}}{\partial M_{j'}^{K}} \right) \right]^2 \sigma^2_{M_{j'}^{K}} \quad (13)$$

$$= \left(\frac{1}{4\pi a^2 \rho_w} \right)^2 \sum_{j'=1}^{N^K} \left[\sum_{j''=1}^{M} \sum_{l=0}^{\infty} \sum_{m=0}^{l} \wp_{ij'j''lm} \right]^2 \sigma^2_{M_{j'}^{K}}, \quad (14)$$

with

$$\wp_{ij'j''lm} = w_l^2 A_{i,j''}^{-1} \left(\Delta c_{lm}'^{j''} \cos m\phi_{j'}'^{K} + \Delta s_{lm}'^{j''} \sin m\phi_{j'}'^{K} \right) \times \tilde{P}_{lm}\left(\cos \theta_{j'}^{K} \right). \quad (15)$$

The computations of variances using Eq. (13) need the error variances of the DPMA or the square roots (sigmas) as input. The error variances for the estimates of TWS, SM and SWE changes at all the mascons are calculated in different ways, see section A.1 of Supplementary material and Step 1 of section 2.3.3.

As shown above, the approach used to assess the error of GWS change is to let the errors of the related factors for TWS, SM, ICE, SWE, LAKE, PM and GIA propagate into that of GWS. Another approach widely used in hydrology is to check the closure of the budget (TWS = GWS + SM + ICE + SWE + LAKE + PM + GIA). Since the closure of the budget has been already considered as a constraint in Eq. (7) or Eq. (11), this approach cannot be used in this study.

Since the reliable Stokes coefficients from GRACE models are given within degree/order 60, in this study, the SH coefficients for the TWS change and the hydrology contributions as well as the GIA effect to be removed are simultaneously used up to degree/order 60. Gaussian filtering is used in the mascon fitting to reduce the effects of high degree/order errors.

2.3. Basic procedure for mascon fitting

In this study, monthly SH coefficients can be computed for TWS, SM and SWE, for multiple sources while the trend rates of the SH coefficients and the DPMA sigmas are available for ICE, LAKE, PM, and GIA from only single source. In the following, we consider the combined usage of two different types of data (i.e., monthly data and trend-rate data), and propose a general procedure for mascon fitting in order to estimate the GWS changes, the trends and their uncertainties in the selected regions of interest. The details for the data and the individual processing are found in the section A of Supplementary material.

2.3.1. Signal leakage precaution

To assure that the data directly used for the inversion include as little as possible leakage signals from outside of our study area, we enlarge the area by 5 degrees outwards. In addition, a synthesis for TWS changes and GIA effects for degrees/orders up to 60 with formulas Eq. (2) gives the results for DPMA at $1^\circ \times 1^\circ$ grids of the enlarged study area, which are then decomposed into SH coefficients up to degree/order 60 with Eq. (5); for the changes of SM, ICE, SWE, LAKE, and PM similar decompositions are done with the corresponding models or observed data.

2.3.2. Mascon setting in the enlarged area

The monthly SH coefficients of the TWS, SM, and SWE changes are given by the mean estimates from the responding multiple sources, the trend together with annual and semiannual terms are obtained by linear regression. The results together with those for other TWS components and the GIA effect are used in a synthesis with Eqs. (6) and (7) to give the SH GWS changes in the enlarged study area, which are the basis for setting mascons. Another criterion is the drainage basin that can contain one or more mascons. The area of one mascon chosen is usually not less than 100000 km^2 due to the limited resolution of the GRACE gravity models. After the mascons are chosen, mascon SH coefficients are computed for each mascon with Eq. (5).

2.3.3. Mascon fitting

The new SH coefficients from section 2.3.1 can be used to calculate the monthly changes and the trends at mascons for TWS and the components, and GIA effect. The error sigmas at mascons can be calculated with the DPMA sigmas for ICE, LAKE, PM and GIA, or with different ways for TWS, SM and SWE. The steps are described as follows:

Step 1. For SM and SWE, the new monthly SH coefficients for multiple sources are used in Eq. (9) to produce the corresponding monthly changes (in EWT) at mascons. The monthly changes as the final estimates and the error sigmas are given at mascons by the mean values and standard deviations among the multi-models used respectively, avoiding any implicit assumption in Eqs. (13) and (14) that the DPMA errors in neighboring discretized masses of Eq. (5) are uncorrelated. For the above calculated monthly changes, the trends and error sigmas at mascons are given by the linear regression method as stated above. Similarly, the monthly TWS changes, the trend rates and the error sigmas at mascons can be calculated, except that the error sigmas at mascons for monthly TWS changes are estimated in a different way (section A.1 of Supplementary material).

Step 2. For ICE, LAKE, PM, and GIA, since their trend rates are given, they are treated differently than SM and SWE. For these four cases, the new monthly SH coefficients are also used in Eq. (9) to produce the corresponding trend rates (in EWT) at mascons. The DPMA error sigmas are prepared according to the observed errors or assumed errors (sections A.2.2∼A.2.4 and A.3 of Supplementary material), and are used in Eq. (14) to give the error sigmas at mascons. The trends at mascons are given by the products of their trend rates with the time from the first month (January 2003) and the error sigmas are produced by relevant propagation of the trend-rate errors.

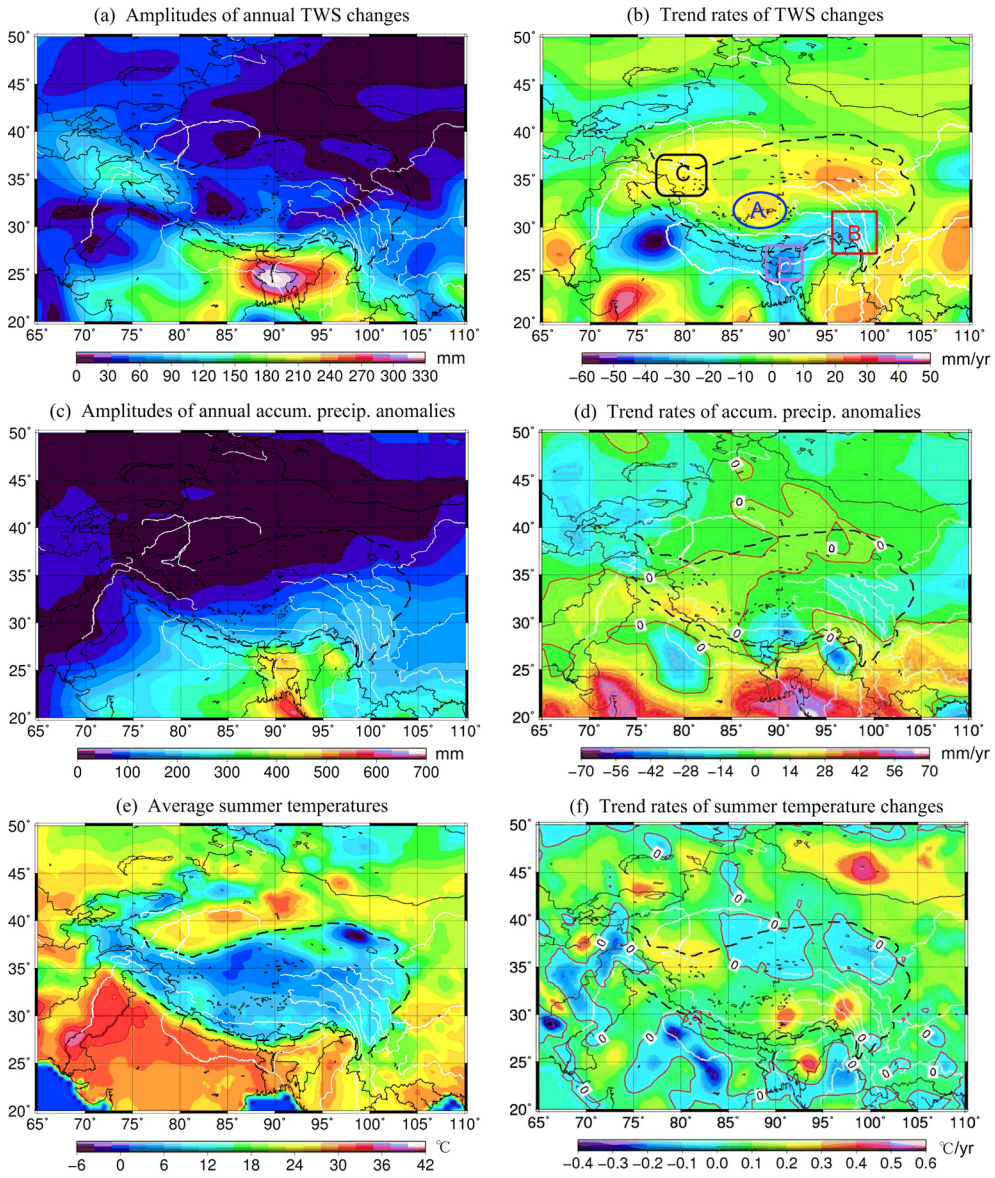

Fig. 2. SH TWS changes compared with precipitations and summer air temperatures from 2003 to 2009 in the study area. The annual amplitudes (a) and trend rates (b) for TWS changes are derived from monthly GRACE data by CSR, GFZ and JPL (Bettadpur, 2012). The annual amplitudes (c) and trend rates (d) for precipitation changes are derived from the monthly accumulated precipitation anomalies from the GPCP model (Adler et al., 2003). The average values (e) and trend rates (f) for summer temperature during the surveyed period are based on the monthly 2-m high air temperature data (Fan and Van den Dool, 2008). The dashed lines delimit the range of the Tibetan Plateau, and A, B, C and D are defined in Fig. 3. Here, anomalies mean the monthly precipitation deviations from the average during the surveyed time.

Step 3. Using the above estimates of monthly changes, trend rates and the error sigmas at masons for TWS, the components (except for GWS), and GIA effect with Eqs. (11) and (12), we have the corresponding estimates for GWS. We provide the uncertainties for the estimates of all the quantities at mascons at the 95% (2 sigma) confidence level.

Since the trend signals are just available and used in this study for ICE, LAKE, and PM, the inverted monthly GWS changes here may include the signals from the seasonal variations of the three hydrology components.

3. Features of the SH changes of TWS, the components and GIA effect

In order to assure the correctness and reasonability of the SH changes of TWS, the components (except for GWS) and GIA effect, they are calculated for the study area by corresponding synthesis. The results are compared with precipitation and air temperature data, and some well water level data and river discharge data, whose features are carefully discussed. In addition, the features for SH GWS trend are compared with those after a 340-km Gaussian filter is used.

3.1. SH TWS changes and the comparisons with precipitation and air temperature data

The fitted annual amplitude and the trends of the SH TWS changes are shown in Fig. 2a, b and compared to precipitation and summer air temperature data (Fig. 2c–f) (see section A.4 of Supplementary material for the data sources and the data processing). In Fig. 2a, a strong annual signal is found to the south of the central and eastern Himalayas, around Bangladesh, while a weaker signal is found to the west of the Tibetan Plateau, around the end of the Upper Indus. The signal amplitudes become smaller from south to north in the Tibetan Plateau. These patterns are simi-

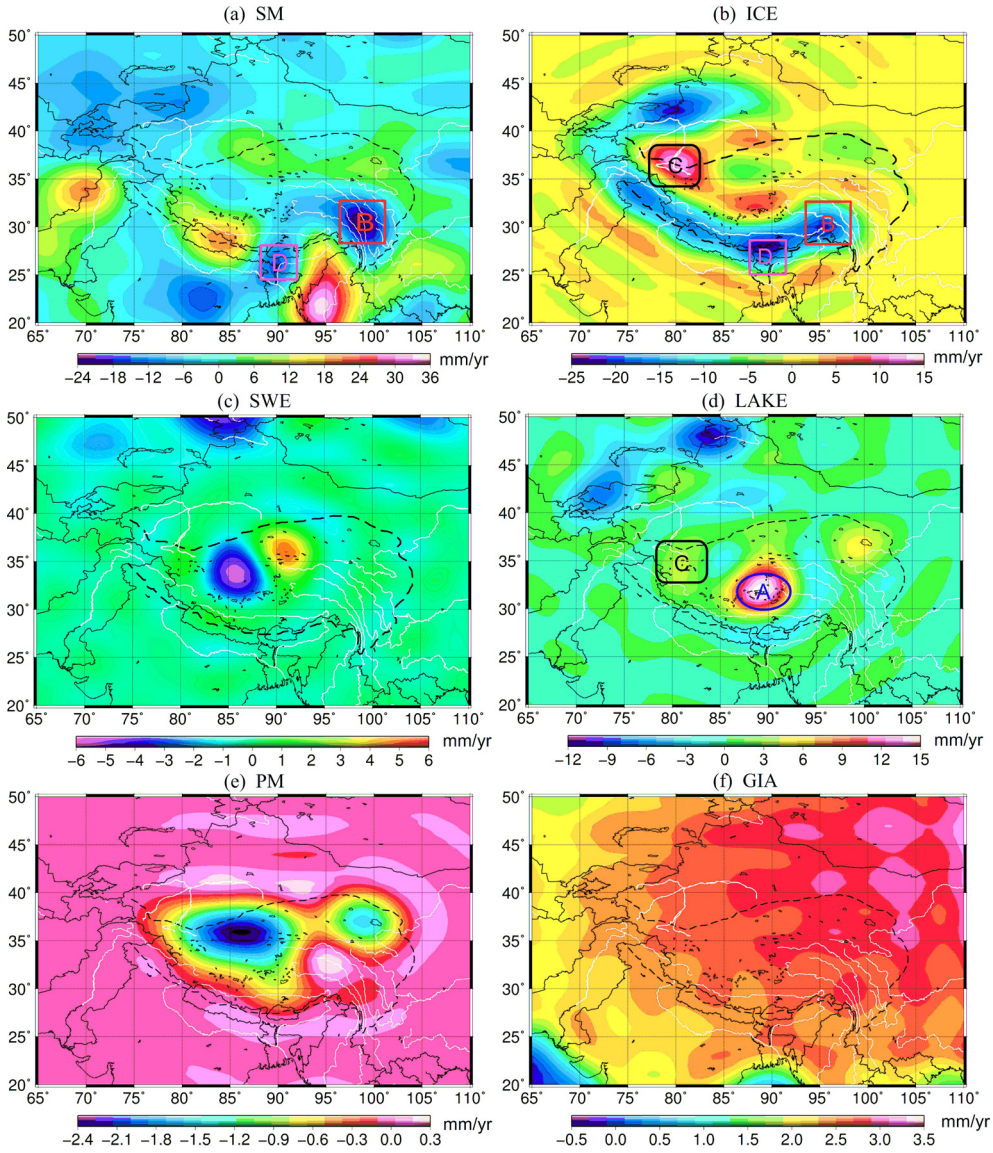

Fig. 3. SH trend rates of TWS components from 2003 to 2009. The data sources used: (a) monthly GLDAS (NOAH/MOSIC/VIC) (Rodell et al., 2004) and CPC data (Fan and van den Dool, 2004), (b) ICESat-1 based glacier measurements (Gardner et al., 2013), (c) monthly GLDAS (CLM/NOAH/MOSIC/VIC) data (Rodell et al., 2004), (d) ICESat-1 lake measurements (Zhang et al., 2011, 2013), (e) one ALD model (Oelke and Zhang, 2007; Erkan et al., 2011) and (f) ICE-6G_C(VM5a) model (Argus et al., 2014; Peltier et al., 2015). A, B, C and D denote positions of the hydrology signals, which will be compared to those when Gaussian filter is used (Fig. A.3).

lar to those found in the annual precipitations (Fig. 2c) showing that the annual TWS changes could be controlled by precipitations. In Fig. 2b, the decreasing trends of SH TWS changes are found along glacier mountain ranges (except for West Kunlun) due to glacier mass loss (as shown in Fig. 3b) and are also basically in accordance with those for precipitations, particularly in the Tien Shan (Fig. 2d). In Fig. 2e, the 7-yr average summer air temperatures at 2-m high are usually positive in glacier mountain ranges. Fig. 2f shows that the temperatures are increasing at rates of up to 0.3 °C/yr. This may cause the 7-yr glacier ice melting (Fig. 3b). Note that in Fig. 2b, one large scale increasing and two decreasing trends of SH TWS changes appear in the northern Tibetan Plateau with centers at the head of the Yellow River Source Region (YeSR) and the Afghanistan–India–Bangladesh regions, respectively. The former one may be caused by the increased runoff recharges from the melt water in neighboring glacier/snow mountains (Fig. A.5). The latter two are obviously due to excessive use of groundwater for agricultural irrigation (Siebert et al., 2013).

3.2. SH changes of the TWS components

As seen in Fig. 2b, the SH TWS trend rates range from −55 mm/yr to 40 mm/yr. For comparison, the SH trend rates of the 6 TWS components are shown in Fig. 3. The signal ranges are −24∼36 mm/yr for SM, −25∼15 mm/yr for ICE, −6∼6 mm/yr for SWE, −12∼15 mm/yr for LAKE, −2.4∼0.3 mm/yr for PM, and 1.6∼3.2 mm/yr for GIA. The contributions from canopy water (<0.02 mm/yr) are also calculated using the GLDAS model, but these are negligible. The results for soil moisture (Fig. 3a) are found to be correlated with the precipitation trends (Fig. 2d). It can also be seen that the mass loss trends of glacier ice (Fig. 3b) along glacier mountain ranges are influenced by decreases in precipitation and increases in summer air temperature (Fig. 2d, f).

The separated SH GWS changes are shown for annual amplitude and the trend in Fig. 4. In Fig. 4a, two great annual signals (∼180 mm and ∼120 mm of amplitude) are found around Bangladesh and along the Upper Indus basin just southwest to Karakoram, respectively. The former one is induced by strong sea-

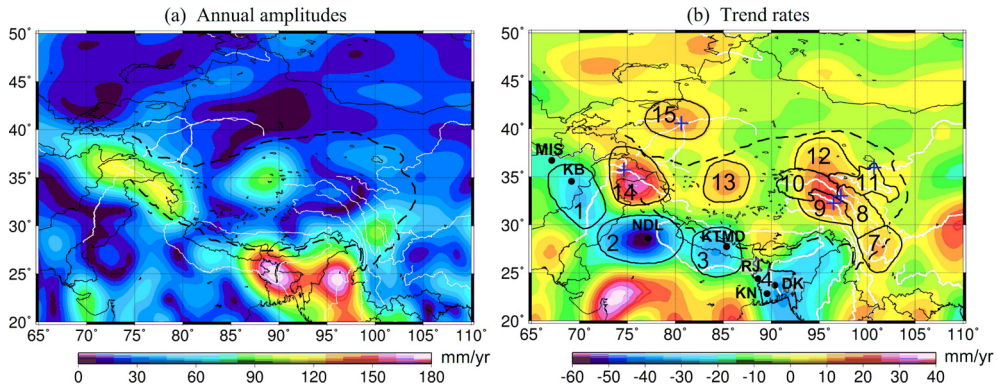

Fig. 4. Annual amplitudes (a) and the trend rates (b) of SH GWS changes from 2003 to 2009. Black dots mark cities with severe groundwater decrease: MIS – Mazar-i-Sharif, KB – Kabul, NDL – New Delhi, KTMD – Katmandu, RJ – Rajshahi, DK – Dhaka, KN – Khulna. The 13 mascons shown are arranged to represent the 12 selected regions of interest. The 5 blue "+" denote the Partab Bridge of the Upper Indus (14), Lower Aksu River (15), Xiangda station (9), Zhimenda station (10), and Tangnaihai station (11) respectively, which are all located near to the discharge terminal of the river basins. The accumulated river discharge anomalies are shown in Fig. 7 and Fig. A.2.

sonal precipitations (Fig. 2c), and the latter mainly due to the seasonal runoffs recharged by adjacent ice/snow melting since the precipitation amount is very small there. In Fig. 4b, there are four positive trend signals mainly in the Jinsha River basin–Three Rivers Source Region (TRSR)–Qaidam basin, central Qiangtang basin, Upper Indus basin and Aksu River basin, respectively, and four negative trend signals distributed mainly along Afghanistan, Pakistan, North India and Bangladesh. The value ranges for SH GWS trend rates are −52∼30 mm/yr for our examined land regions. Accordingly, the contributions from GWS, SM, ICE and LAKE together dominate in the SH TWS trend (Fig. 2b).

In Fig. A.1, the monthly SH changes of TWS and the components, as well as the GIA effect are shown. They are much correlated between TWS, SM and GWS in most regions, and the contributions of GWS and soil moisture dominate in the monthly SH TWS changes. The SH ICE trends dominate among the trends for ICE, LAKE and GIA for all the 12 regions. Prominent SH SWE changes only occur in mascon 10 (Yangtze River Source Region (YaSR)) and mascon 13 (central Qiangtang basin). Note that there are larger trend rates of ice mass loss in mascon 9 (Nujiang-Lancangjiang Rivers Source Region (NLSR)), mascon 14 (Upper Indus basin) and mascon 15 (Aksu River basin).

The monthly SH GWS changes are shown in Fig. A.2 for 7 cities in or near our signals 1 to 4 (as shown in Fig. 4b). In the cities Mazar-i-Sharif (Fig. A.2a), New Delhi (Fig. A.2c), Khulna (Fig. A.2f) and Dhaka (Fig. A.2g), declining trends of groundwater levels are found and validated by many sources (e.g., Muradi et al., 2013; Wada et al., 2010; Correspondent, 2015; Hoque et al., 2007). In the cities Kabul (Fig. A.2b), Kathmandu (Fig. A.2d) and Rajshahhi (Fig. A.2e), monthly SH GWS changes show agreement with those from well data (Mack et al., 2013; Gautam and Prajapati, 2014 and Abdullah Aziz et al., 2015). In addition, in the Upper Indus basin (Fig. A.2h) the monthly SH GWS changes agree well to estimates of yearly accumulated river discharge anomalies from 2003 to 2008 at the Partab Bridge gauge (Cook et al., 2013).

3.3. Effects of Gaussian filtering on the SH changes of TWS and the components

In Fig. 2b, there are four isolated signals: the one labeled A in the Endorheic basin of the Tibetan Plateau (Fig. A.5) is related to mass gain of lake water (see A in Fig. 3d), B is due to mass loss of soil moisture and glacier ice in the East Nyainqêntanglha and Hengduan Mountains (see B in Fig. 3a, b), C is due to mass gain of glacier ice and lake water in the west Kunlun Mountains (see C in Fig. 3b, d), and D is due to mass loss of soil moisture and glacier ice in the region from North Bangladesh to the Himalayas (see D in Fig. 3a, b). However, if a 340-km Gaussian filter is used as in Fig. A.3a, the four independent signals are smoothed or even seem to disappear for A, B and C.

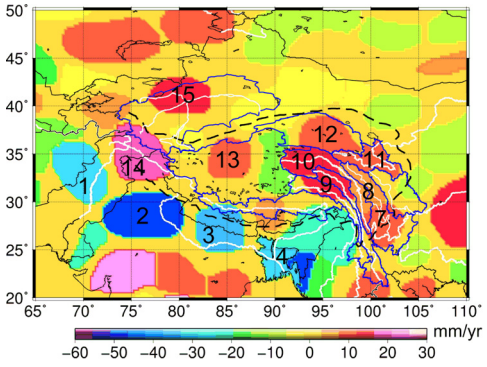

Fig. 5. Trend rates of GWS changes from 2003 to 2009 inverted for all the mascons in the study area. Blue lines delimit the basins. There are 12 regions of interest: 1 – Afghanistan–Pakistan, 2 – Northwest India, 3 – north-central India, 4 – Bengal basin of Bangladesh, 7+8 – Jinsha River basins, 9 – NLSR, 10 – YaSR, 11 – YeSR, 12 – Qaidam basin, 13 – the central Qiangtang Nature Reserve, 14 – Upper Indus basin adjacent to West Himalaya, 15 – Aksu River basin. The Endorheic basin is to the west of the mascon 10 (YaSR).

Comparison of the GWS trend (Fig. 4b) with the Gaussian filtered one (Fig. A.3h) shows that the filtering not only smoothes the signals but also shifts the locations of the signals in Fig. 4b. The effects to signals with the numbers 1, 2, 3, 13, 14 and 15 are particularly prominent: they are independently distributed in Fig. 4b and are mixed at the borders when the filter is used (Fig. A.3h). Thus, it is reasonable to use the SH GWS trend for the mascon setting instead of that with a 340-km Gaussian Filter.

4. Inverted results and analysis for GWS changes in the 12 selected regions

The data and models described in section A of Supplementary material are used to generate corresponding SH coefficients and DPMA error sigmas, which are used for mascon fitting inversion. Here, we focus on showing the estimates of monthly changes and trend rates, and the uncertainties of TWS, the components (including GWS), and GIA effect with added discussion.

4.1. Mascon fitting inversion

The anomalies of SH GWS trend (Fig. 4b), where the Gaussian filter is not used, are then the bases to determine the positions

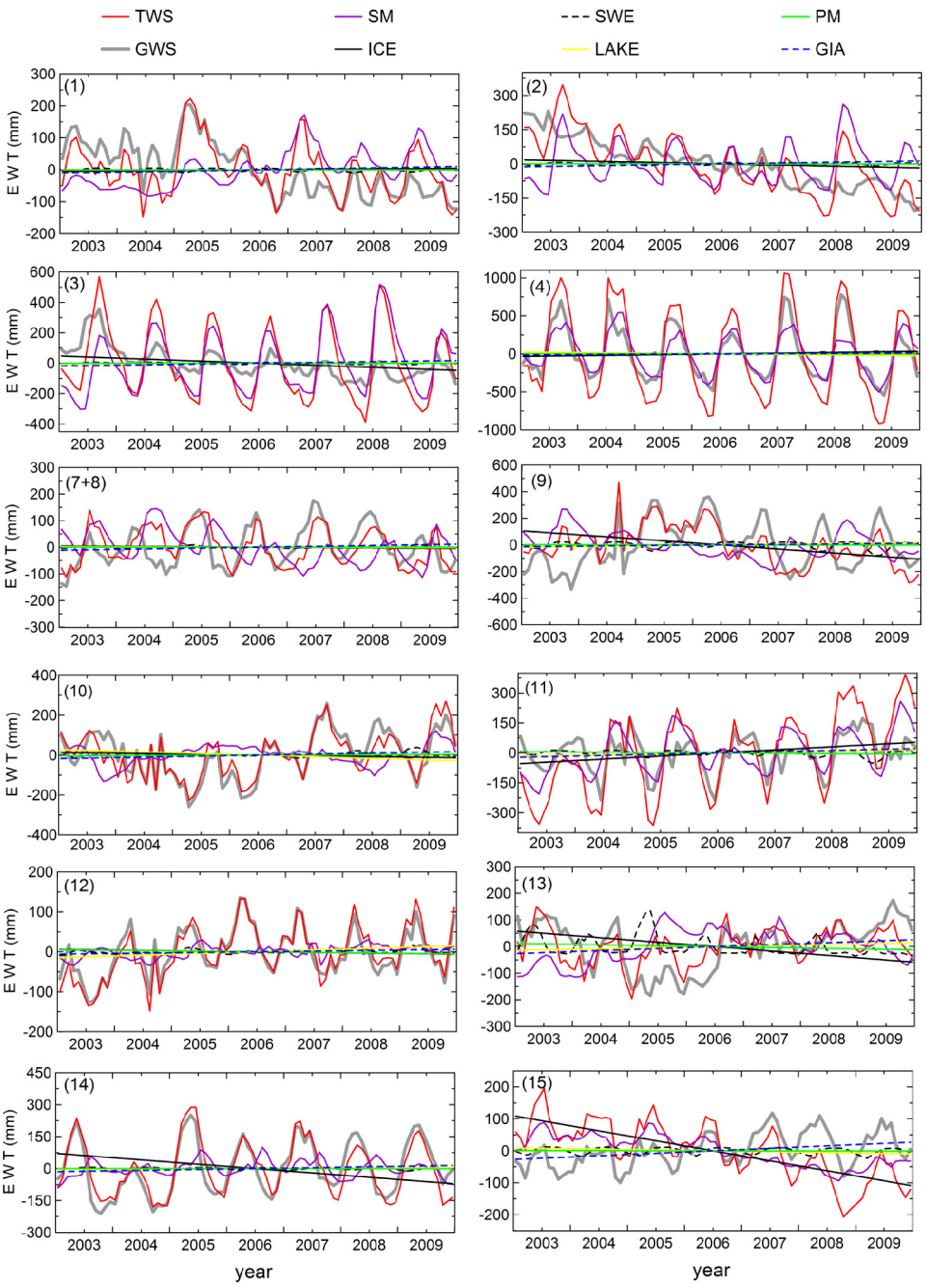

Fig. 6. Monthly changes of TWS and the hydrologic components as well as the GIA effect from 2003 to 2009 inverted for 12 selected regions. Note that the results for PM, ICE, and LAKE are given by their trends.

and ranges of the mascons in the enlarged study area. In addition, the distribution of some drainage basins (e.g., the river source regions in the eastern plateau, and the Bengal basin of Bangladesh) are also considered for mascon setting. A total of 70 mascons are determined, in which only those in our study area are shown in Fig. 4b and Fig. 5. The 12 selected regions of interest are delimited by mascons: 1 – Afghanistan–Pakistan, 2 – Northwest India, 3 – north-central India, 4 – Bengal basin of Bangladesh, 7+8 – Jinsha River basin, 9 – NLSR, 10 – YaSR, 11 – YeSR, 12 – Qaidam basin, 13 – the central Qiangtang Nature Reserve, 14 – Upper Indus basin adjacent to West Himalaya, 15 – Aksu River basin.

Although the GWS changes estimated from mascon fitting inversion are available for all the mascons in the surveyed area (e.g., in Fig. 5 for their trends), they are shown in Figs. 6 and 7 and Table A.2 only for the 12 selected regions. It is found that the 'observed' monthly Gaussian filtered SH GWS changes match the calculated signals very well. Here, taking the SH GWS trends for example, the 'observed' signals in Fig. A.3h are compared with the calculated signals (Fig. A.4a) to give very small residues with magnitudes of ∼0.8 mm/yr. This shows that the inversion can better restore the 'observed' signals and in this sense the inversion results are reasonable.

4.2. Corrections for the estimates of GWS changes

In Fig. 6, the changes of TWS and its components, and GIA effect are also attached in order to find the relative importance of the corresponding corrections for the estimates of GWS changes.

The monthly changes of TWS, GWS and SM are basically correlated. The corrections for the SM contributions (SM corrections)

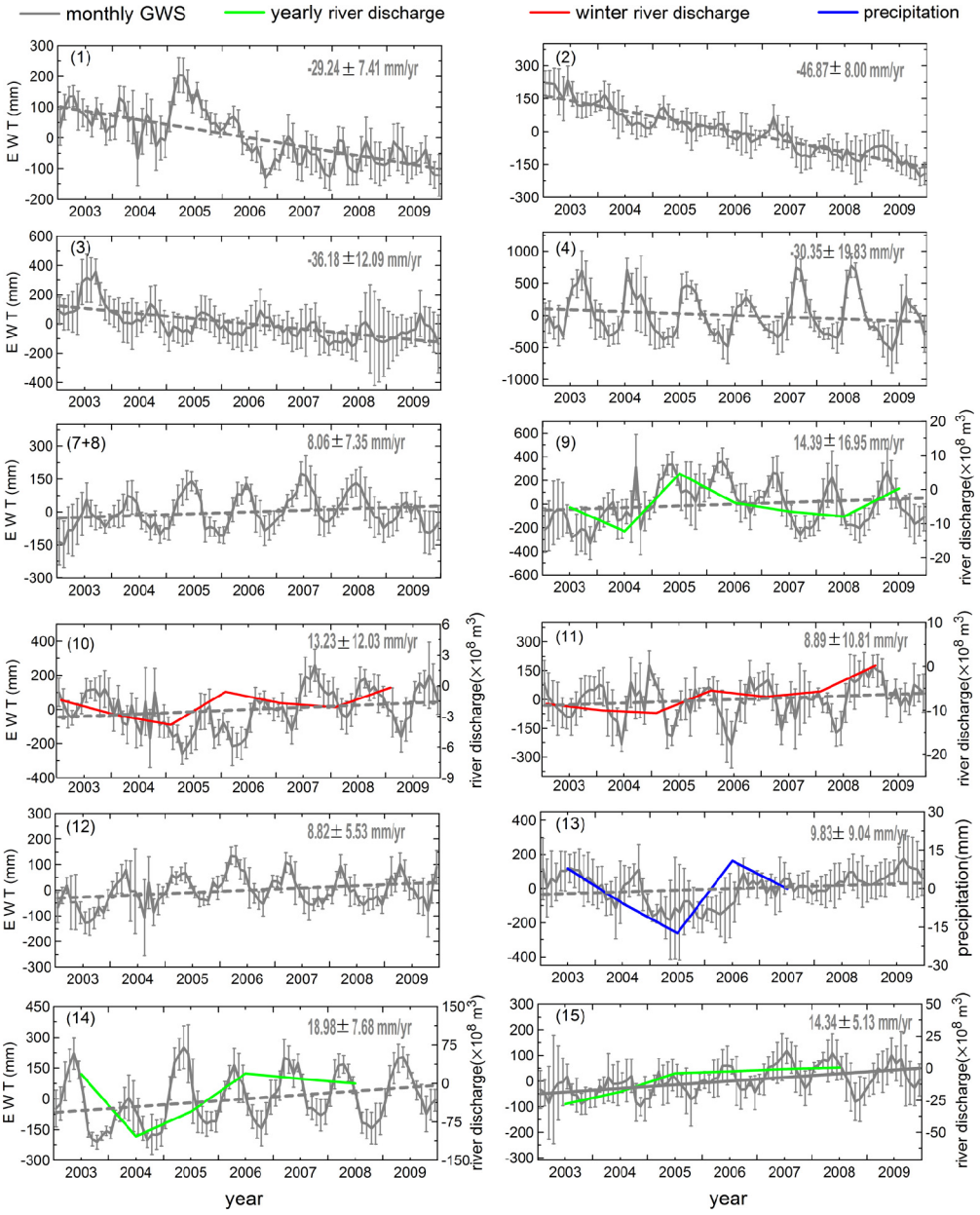

Fig. 7. Inverted monthly GWS changes and trend rates with uncertainties and comparison with observed data from 2003 to 2009 in the selected 12 regions. The thick grey curves denote the monthly GWS changes, the dashed grey lines and grey numbers show the trends and the trend rates. Uncertainties use 2 error sigma and the length of each error bar is the quadruple error sigma. Winter (December, January, February, March) accumulated discharge anomalies are shown for mascon 10 at Zhimenda station of the YaSR and for mascon 11 at Tangnaihai station of the YeSR (Sun et al., 2015). Yearly accumulated discharge anomalies are shown for mascon 9 at Xiangda station of Lancangjiang River Source (Sun et al., 2015), for mascon 14 at the Partab Bridge of the Upper Indus (Cook et al., 2013), and for mascon 15 in lower Aksu River (Ling et al., 2011). Yearly accumulated precipitation anomalies are shown for mascon 13 in the central Qiangtang Nature Reserve (Li et al., 2010). Here, anomalies mean the winter or yearly discharge deviations from the average during the surveyed time.

are usually most important for the separation of GWS signals from TWS signals. ICE corrections are also important for mascons 9, 11, 13, 14 and 15. LAKE corrections should be applied especially for mascons 10, 12, 13 and 15. Significant PM corrections yield for mascons 11 and 13. The GIA corrections are found to be as much as ~1.0 Gt/yr for most mascons resulting in a larger contribution than that for SWE and PM, and partly LAKE. Nonetheless, the ICE, LAKE, PM and GIA corrections together are usually important for the estimates of GWS trends (Table A.2).

One reason for the remarkable GIA correction is that the new GIA model ICE-6G_C (VM5a) considers the rotational feedback effects to predict the additional SH geoid anomalies (degrees/orders up to 0 ~ 60) with the four quadrant distributions. One quadrant is located around the site (100°E, 47°N) in the northeastern part of our study area with an amplitude of 0.10~0.21 mm/yr, corresponding to EWT amplitudes of 1.6~3.2 mm/yr (Fig. 3f).

Finally, we note that the estimated signals of TWS and the components (except for GWS) shown in Fig. 6 and Table A.2 are sometimes caused by signal leakage from outside of the mascon.

4.3. Estimates of GWS changes in the 12 regions and comparison to ground data

4.3.1. Estimates of GWS changes and uncertainties

The estimates of GWS changes and trends in the 12 regions are shown in Fig. 7 and listed in Table A.2. The uncertainties rigorously take into account the measurement errors for GRACE data, ice melting and lake measurements, model variability or model er-

rors (for SM, SWE, PM and GIA). As shown in Fig. 7 and Table A.2, the estimates are usually robust when compared with the uncertainties.

In Fig. 7, we explicitly show the intra-annual (seasonal) and interannual variations. The maximal and minimal magnitudes for seasonal signals are found in mascon 4 (Bengal basin of Bangladesh) and mascon 12 (Qaidam basin) due to strong and weak precipitations, respectively (e.g., Shamsudduha et al., 2012). As stated before, monthly GWS changes may include the seasonal variations of ICE, LAKE and PM.

As seen in Table A.2, the TWS errors are the biggest error sources for the estimates of GWS trend rates, resulting from the errors of GRACE data. The SM correction errors are most prominent among those for other TWS components due to largest variability of the models available. The ICE, LAKE and GIA correction errors are similar for most mascons. The PM correction errors are only important for mascons 10 to 13, while the SWE correction errors are large for mascons 9 and 13.

As shown in Figs. 5 & 7, and Table A.2, we find that the GWS changes have increasing trends in the regions of the Jinsha River basin, NLSR, YaSR, YeSR, the Qaidam basin, the central Qiangtang Nature Reserve and the Aksu River basin. The rates are $+2.46 \pm 2.24$ Gt/yr, $+1.77 \pm 2.09$ Gt/yr, $+1.86 \pm 1.69$ Gt/yr, $+1.14 \pm 1.39$ Gt/yr, $+1.52 \pm 0.95$ Gt/yr, $+1.66 \pm 1.52$ Gt/yr, $+5.37 \pm 2.17$ Gt/yr and $+2.77 \pm 0.99$ Gt/yr, respectively. Possible causes are discussed in the next section.

4.3.2. Discussion

For the comparison to ground data, we focus on those regions where new GWS trend signals are found in this study. Since the observations for GWS changes in such regions are scarcely made and reliable hydrology models for GWS prediction are not available, here we turn to river discharge data, precipitation data, air temperature, as well as limited water level data or reported news to support our results. In addition, the hydrologic and hydrogeologic conditions are also discussed.

Mass losses in the trends for mascons 1 to 4 (Afghanistan–India–Bangladesh) in Fig. 7 are induced by the excessive use of groundwater (Muradi et al., 2013; Mack et al., 2013; Gautam and Prajapati, 2014; Abdullah Aziz et al., 2015; Correspondent, 2015; Ahmad, 2011; Hoque et al., 2007 and Siebert et al., 2013).

The mass gains in mascons 7+8 (Jinsha River basin) in Fig. 7 are likely caused by increased precipitations for the lower Jinsha River basin (Fig. 2d) and increased recharges in the upper reach by melt water of the glaciers/snow-caps and permafrost of the Hengduan Mountains (HDM) (Fig. 3b, e, Fig. A.5) under the condition of increased air temperature (Fig. 2f).

The mass gains found for mascons 9, 10 and 11 (Nujiang River Source Region (NuSR) and TRSR) in Fig. 7 are compared with simultaneous river discharge data showing good agreement for the trends. Especially, the winter discharge data are more valuable for the YaSR and YeSR since they can more directly reflect the groundwater changes; the comparison results are then persuasive. The mass gains found in the four river basins could be caused by increased recharges by melt water of the glaciers/snow-caps and permafrost of Nyainqêntanglha (NQT), Tangula Mountains (TGL), Bayan HAR Mountains (BYH), Kunlun Mountains (KLM) and Anyemaqen Range (Fig. 3b, e) with increased air temperature (Fig. 2f). Since the regionally decreased precipitations (Fig. 2d) and increased permafrost degradation (Fig. 3e) due to air temperature increase (Fig. 2f) may cause the mass losses of GWS, more recharges are probably required for these four regions. We propose one additional cause, groundwater seepages flowing from the Endorheic basin to the west of TRSR through fault tunnels in deep aquifers (Fig. A.5), based on three reasons: NuSR and TRSR are linked with the Endorheic basin by several large active faults, even the NuSR is linked to the Lake Nam Co and Lake Serling Co of the Endorheic basin; there are already some evidences that show that the waters in the Endorheic basin discharge to regions outside (Chen and Wang, 2012; J.S. Chen et al., 2014; Zhou et al., 2013 for Lake Nam Co). However the hypothesis needs to be further studied (e.g., by isotopes tracing of groundwater).

In order to protect the ecological environment in the TRSR, China has been implementing the Ecological Protection and Construction Project since 2005 in the region. Through eco-migration, grazing ban, forest and wetland reservation, artificial precipitation (counting to 26 Gt till 2009), rat control etc., the ecological environment has been improved significantly, and the water conservation ability also has got improved (Shao et al., 2013), which may have increased the GWS in the TRSR.

In view of our results one should have a closer look into the hydrologic and hydrogeologic environments for the river source regions in the eastern plateau (see also Cheng and Jin, 2013). The river source regions are delimited basically by large mountains: Kunlun, Anyemaqen, Bayan Har, Tanggula and Nyainqêntanglha (Fig. A.5). The altitudes of an average ∼4500 m decrease from northwest to southeast, whereas precipitation decreases as well while air temperature increases and the ALD increases towards the lower land and valleys. In the TRSR, the widely distributed thick carbonates, clastic rocks and/or the combinations contain pores, fissures and karst caves that soundly stores groundwater (Institute of Hydrogeology and Geology (IHEG) National Bureau of Geology, 1979). Since the permafrost has a mosaic distribution, the effective aquifers are deep and widespread, and thus contain plentiful of water (Cheng and Jin, 2013). According to Wang et al. (1990), the cycling time of groundwater here is relatively short, due to the high elevations, rugged terrains, steep groundwater gradients (e.g., with respect to the terminal of YaSR, the start of Yangtze River is ∼1000 m high and the Nam Co is ∼500 m high). The cycling time is 1∼4 yr for supra-permafrost water and ∼30 yr for sub-permafrost water. The large active faults (Liu et al., 1989) may further speed up the transport of groundwater in depth. According to a recent study (Gleeson et al., 2016), the thickness of groundwater in the river basins can be ∼1 m for cycling time less than 50 yr, which is far larger than our estimates of annual signals and 7-year trend signals for GWS changes, showing the possibility that the groundwater could change as seen in our estimates (Fig. 7 and Table A.2).

Mass gain in mascon 12 (Qaidam basin) (Fig. 7) could be due to increased recharges by melt water of the glaciers/snow-caps/permafrost and precipitations in KLM and Qilian Mountains (QLM) (Fig. 3b, e, Fig. 2d).

The transition in 2005 from mass loss to gain is found for mascon 13 (the central Qiangtang Nature Reserve) (Fig. 7), and is also seen in the precipitation data (Li et al., 2010). It is due to the simultaneous precipitation changes (Fig. 2d) and increased recharges by melt water (Fig. 3b) and precipitation from KLM.

Mass gains are found for mascons 14 to 15 (Upper Indus basin and Aksu River basin) (Fig. 7) and are supported by river discharge increase found at the Partab Bridge of the Upper Indus (Cook et al., 2013) and at the lower reach of Aksu River south to the central Tien Shan (Ling et al., 2011). Mass gains could be due to the increased runoff recharges by melt water of the glaciers/snow-caps and permafrost of West Himalayas, Karakoram and Tien Shan (Fig. 3b).

Our results for mascons 1 to 4 basically agree well with previous estimates. For Northwest India (mascon 2), our estimate is -17.95 ± 3.06 Gt/yr (2003–2009) while previous estimates are: -17.7 ± 4.5 Gt/yr (2002.08–2008.10) by Rodell et al. (2009), -20.4 ± 7.1 Gt/yr (2003.01–2012.12) by J.L. Chen et al. (2014) and ∼−20.2 Gt/yr (2003.01–2012.12) by Yi and Sun (2014). For Bengal

basin of Bangladesh (mascon 4), our estimate of -4.36 ± 2.85 Gt/yr is compatible with the upper bound estimate of -2.83 ± 0.42 Gt/yr (2003–2007) by Shamsudduha et al. (2012), after an additional total contribution of 1.1 Gt/yr is corrected from SWE, ICE and LAKE in the plateau and from the GIA model. For Afghanistan–India–Bangladesh (mascons 1 to 4 and related mascons), our total estimate is -53.3 ± 7.60 Gt/yr, which is close to the value -54.0 ± 9.0 Gt/yr (2002.04–2008.06) by Tiwari et al. (2009). The differences found above are mainly due to the use of new GRACE data and the improved GIA model, our reasonable consideration for the contributions of glacier ice melting, lake water changes etc., the unique mascon setting and a different surveyed time span.

5. Conclusions

Satellite gravity data were used together with multiple hydrology models and data, and a GIA model to separate groundwater changes in the Tibetan Plateau and adjacent areas during the period from 2003 to 2009. To improve the quality and accuracy of estimates, we used updated Release-5 GRACE data, glacier ice budgets and lake-level data measured by ICESat-1, and an improved GIA model as well as a permafrost ALD model together with a mascon inversion.

The 7 year GWS decreasing trend rates due to groundwater depletion are found to be -8.36 ± 2.12 Gt/yr for Afghanistan–Pakistan, -17.95 ± 3.06 Gt/yr for Northwest India, -8.82 ± 2.95 Gt/yr for north-central India, and -4.36 ± 2.85 Gt/yr for the Bengal basin of Bangladesh, which agrees well with previous estimates.

The GWS increasing trend rates during the surveyed period are found to be $+2.46 \pm 2.24$ Gt/yr for the Jinsha River basin, $+1.77 \pm 2.09$ Gt/yr for the NLSR, $+1.86 \pm 1.69$ Gt/yr for the YaSR, $+1.14 \pm 1.39$ Gt/yr for the YeSR, $+1.52 \pm 0.95$ Gt/yr for the Qaidam basin, $+1.66 \pm 1.52$ Gt/yr for the central Qiangtang Nature Reserve, $+5.37 \pm 2.17$ Gt/yr for the Upper Indus basin and $+2.77 \pm 0.99$ Gt/yr for the Aksu River basin. Increased runoff recharges from surrounding glaciers/snow-caps, permafrost and/or precipitations are the likely cause for groundwater increase in all the regions. For the TRSR, the Chinese Ecological Protection and Construction Project successfully helps in keeping the groundwater, and seepages from the Endorheic basin to the west could be a contributor for more water, which however requires further intensive studies.

The measurement errors from GRACE gravity data and the variability of soil moisture models used are found to contribute to most of the uncertainties of the estimates for GWS changes.

Our new findings for the GWS changes especially in the eastern Tibetan Plateau, the Upper Indus basin and the Aksu River basin provide useful information for developing regional agriculture, animal husbandry, and ecological restoration in these areas.

Acknowledgements

We thank C.K. Shum for discussion that led to this study. Yafei Sun, Yongling Sun, Lin Liu and Guocheng Wang are thanked for their kind help on data collection and plot drawing. We also thank Kosuke Heki and an anonymous reviewer for their very helpful comments and suggestions. Some figures are drawn with the GMT software. Hansheng Wang is supported by National Natural Science Foundation of China (Grant Nos. 41431070, 41590854, 41174016, 41274026), National Key Basic Research Program of China (973 Program, grant No. 2012CB957703) and the CAS/SAFEA International Partnership Program for Creative Research Teams (Grant No. KZZD-EW-TZ-05). Patrick Wu is supported by Hong Kong Research Grants Council–General Research Fund grant 17305314. Liming Jiang is supported by Hundred Talents Program of the Chinese Academy of Sciences and National Natural Science Foundation of China (Grant Nos. 41274024, 41321063).

Appendix A. Supplementary material

Supplementary material related to this article can be found online at http://dx.doi.org/10.1016/j.epsl.2016.06.002.

References

Abdullah Aziz, M., Abul Kashem Majumder, M., Shahjahan Kabir, Md., Ismail Hossain, Md., Farhat Rahman, N.M., Rahman, F., Hosen, S., 2015. Groundwater depletion with expansion of irrigation in Barind Tract: a case study of Rajshahi District of Bangladesh. Int. J. Geol. Agric. Environ. Sci. 3, 32–38.

Adler, R.F., Huffman, G.J., Chang, A., Ferraro, R., Xie, P., Janowiak, J., Rudolf, B., Schneider, U., Curtis, S., Bolvin, D., Gruber, A., Susskind, J., Arkin, P., 2003. The version 2 Global Precipitation Climatology Project (GPCP) monthly precipitation analysis (1979–present). J. Hydrometeorol. 4, 1147–1167.

Ahmad, R., 2011. Dhaka's groundwater drops 6 m in 7 years. The Daily Star, October 25, 2011. See: http://archive.thedailystar.net/newDesign/news-details.php?nid=207870.

Argus, D.F., Peltier, W.R., Drummond, R., Moore, A.W., 2014. The Antarctica component of postglacial rebound model ICE-6G_C (VM5a) based upon GPS positioning, exposure age dating of ice thicknesses, and relative sea level histories. Geophys. J. Int. 198 (1), 537–563.

Bettadpur, S., 2012. UTCSR level-2 processing standards document for level-2 product release 005. Center for Space Research, University of Texas at Austin.

Chen, J.L., Li, J., Zhang, Z.Z., Ni, S.N., 2014. Long-term groundwater variations in Northwest India from satellite gravity measurements. Glob. Planet. Change 116, 130–138.

Chen, J.S., Wang, Q.Q., 2012. A discussion of groundwater recharge source in arid areas of North China. Water Res. Prot. 28 (3), 5–8.

Chen, J.S., Chen, X.X., Wang, T., 2014. Isotopes tracer research of wet sand layer water sources in Alxa Desert. Adv. Water Sci. 25, 196–206.

Cheng, G.D., Jin, H.J., 2013. Permafrost and groundwater on the Qinghai–Tibet Plateau and in northeast China. Hydrogeol. J. 21 (1), 5–23.

Cook, E.R., Palmer, J.G., Ahmed, M., Woodhouse, C.A., Fenwick, P., Zafar, M.U., Wahab, M., Khan, N., 2013. Five centuries of Upper Indus River flow from tree rings. J. Hydrol. 486, 365–375.

Correspondent, 2015. Groundwater depletion threatens water supply in Khulna. Dhaka Tribune, March 30, 2015. See: http://www.dhakatribune.com/bangladesh/2015/mar/30/groundwater-depletion-threatens-water-supply-khulna.

Döll, P., Kaspar, F., Lehner, B., 2003. A global hydrological model for deriving water availability indicators: model tuning and validation. J. Hydrol. 270, 105–134.

Erkan, K., Shum, C.K., Wang, L., Jekeli, C., Lee, H., Panero, W.R., Duan, J.B., Huang, Z.W., Wang, H.S., 2011. Geodetic constraints on the Qinghai–Tibetan Plateau present-day geophysical processes. Terr. Atmos. Ocean. Sci. 22 (2).

Fan, Y., Van den Dool, H., 2008. A global monthly land surface air temperature analysis for 1948–present. J. Geophys. Res. 113, D01103.

Fan, Y., van den Dool, H., 2004. Climate Prediction Center global monthly soil moisture data set at 0.5 degree resolution for 1948 to present. J. Geophys. Res. 109, D10102.

Farinotti, D., Longuevergne, L., Moholdt, G., Duethmann, D., Mölg, T., Bolch, T., Vorogushyn, S., Güntner, A., 2015. Substantial glacier mass loss in the Tien Shan over the past 50 years. Nat. Geosci. 8, 716–723.

Gardner, A.S., Moholdt, G., Graham Cogley, J., Wouters, B., Arendt, A.A., Wahr, J., Berthier, E., Hock, R., Tad Pfeffer, W., Kaser, G., Ligtenberg, S.R.M., Bolch, T., Sharp, M.J., Hagen, J.O., van den Broeke, M.R., Paul, F., 2013. A reconciled estimate of glacier contributions to sea level rise: 2003 to 2009. Science 340, 852–857.

Gautam, D., Prajapati, R.N., 2014. Draw down and dynamics of groundwater table in Kathmandu valley, Nepal. Open Hydrol. J. 8, 17–26.

Ge, S., Wu, Q.B., Lu, N., Jiang, G.L., Ball, L., 2008. Groundwater in the Tibet Plateau, western China. Geophys. Res. Lett. 35, L18403.

Gleeson, T., Befus, K.M., Jasechko, S., Luijendijk, E., Cardenas, M.B., 2016. The global volume and distribution of modern groundwater. Nat. Geosci. 9, 161–167.

Haile, K.H., 2011. Estimation of terrestrial water storage in the upper reach of Yellow River. MSc Thesis. University of Twente, Netherlands, pp. 7–11.

Hoque, M.A., Mozzammel Hoque, M., Ahmed, K.M., 2007. Declining groundwater level and aquifer dewatering in Dhaka metropolitan area, Bangladesh: causes and quantification. Hydrogeol. J. 15, 1523–1534.

Institute of Hydrogeology and Engineering Geology (IHEG), National Bureau of Geology, China, 1979. Qinghai province Hydrogeologic Map. In: Hydrogeologic Atlas of People's Republic of China. China Cartographic Publishing House, 41 (in Chinese).

Jacob, T., Wahr, J., Tad Pfeffer, W., Swenson, S., 2012. Recent contributions of glaciers and ice caps to sea level rise. Nature 482, 514–518.

Jarvis, A., Reuter, H.I., Nelson, A., Guevara, E., 2008. Hole-filled SRTM for the globe Version 4. Available from the CGIAR-CSI SRTM 90m Database, http://srtm.csi.cgiar.org.

Jekeli, C., 1981. Alternative methods to smooth the Earth's gravity field. Rep. 327. Dep. of Geod. 557 Sci. and Surv., Ohio State Univ., Columbus.

Jin, S.G., Feng, G.P., 2013. Large-scale variations of global groundwater from satellite gravimetry and hydrological models, 2002–2012. Glob. Planet. Change 106, 20–30.

Kääb, A., Berthier, E., Nuth, C., Gardelle, J., Arnaud, Y., 2012. Contrasting patterns of early twenty-first-century glacier mass change in the Himalayas. Nature 488 (7412), 495–498.

Kääb, A., Nuth, C., Treichler, D., Berthier, E., 2014. Brief Communication: contending estimates of early 21st century glacier mass balance over the Pamir–Karakoram–Himalaya. Cryosphere Discuss. 8, 5857–5874.

Li, L., Yang, X.H., ZhaXi, Y.Z., BaSang, D.Z., 2010. Analysis on the climatic characteristics of the Qiangtang Nature Reserve in Tibet in recent 30 years. Plateau Mt. Meteorol. Res. 30 (1), 62–65.

Ling, H.B., Xu, H.L., Zhang, Q.Q., Shi, W., 2011. The annual runoff variation trends in the three headstreams of Tarim River. Scient. Geogr. Sin. 31 (6), 728–733.

Liu, G., Ma, T., Huang, P., Bai, Y., 1989. Major active faults and their recent movement. In: Ma, X., Ding, G., Gao, W., Zhang, H., Zhang, B., Ma, Z. (Eds.), Lithospheric Dynamics Atlas of China. China Cartographic Publishing House, Beijing China, 17 (in Chinese).

Mack, T.J., Chornack, M.P., Taher, M.R., 2013. Groundwater-level trends and implications for sustainable water use in the Kabul Basin, Afghanistan. Environ. Syst. Decis. 33, 457–467.

Matsuo, K., Heki, K., 2010. Time-variable ice loss in Asian high mountains from satellite gravimetry. Earth Planet. Sci. Lett. 290, 30–36.

Muradi, S., Phien-Wej, N., Giao, P.H., 2013. Depletion of water resources, issues and challenges of water supply management in Mazar-i-Sharif city, Afghanistan. Res. J. Environ. Earth. Sci. 5 (5), 242–251.

Oelke, C., Zhang, T.J., 2007. Modeling the active-layer depth over the Tibetan Plateau. Arct. Antarct. Alp. Res. 39, 714–722.

Peltier, W.R., Argus, D.F., Drummond, R., 2015. Space geodesy constrains ice-age terminal deglaciation: the global ICE-6G_C (VM5a) model. J. Geophys. Res., Solid Earth 120, 450–487.

Rodell, M., Houser, P.R., Jambor, U., Gottschalck, J., Mitchell, K., Meng, C.J., Arsenault, K., Cosgrove, B., Radakovich, J., Bosilovich, M., Entin, J.K., Walker, J.P., Lohmann, D., Toll, D., 2004. The global land data assimilation system. Am. Meteorol. Soc. 85 (3), 381–394.

Rodell, M., Velicogna, I., Famiglietti, J.S., 2009. Satellite-based estimates of groundwater depletion in India. Nature 460 (7258), 999–1002.

Shamsudduha, M., Taylor, R.G., Longuevergne, L., 2012. Monitoring groundwater storage changes in the highly seasonal humid tropics: validation of GRACE measurements in the Bengal Basin. Water Resour. Res. 48, W02508.

Shao, Q.Q., Liu, J.Y., Huang, L., Fan, J.W., Xu, X.L., Wang, J.B., 2013. Integrated assessment on the effectiveness of ecological conservation in Sanjiangyuan National Nature Reserve. Geogr. Res. 32 (9), 1645–1656 (in Chinese).

Siebert, S., Henrich, V., Frenken, K., Burke, J., 2013. Global Map of Irrigation Areas version 5. Rheinische Friedrich-Wilhelms-University, Bonn, Germany / Food and Agriculture Organization of the United Nations, Rome, Italy. (Available at http://www.fao.org/nr/water/aquastat/irrigationmap/index10.stm).

Sun, Y.S., Duan, S.Q., Li, Y., Cao, G.C., 2015. Variation characteristics and trend analysis of runoff at the source regions of the three river in Qinghai during recent years. J. Water Res. Water Eng. 26 (1), 52–57.

Tiwari, V.M., Wahr, J., Swenson, S., 2009. Dwindling groundwater resources in northern India, from satellite gravity observations. Geophys. Res. Lett. 36, L18401.

Wada, Y., van Beek, L.P.H., van Kempen, C.M., Reckman, J.W.T.M., Vasak, S., Bierkens, M.F.P., 2010. Global depletion of groundwater resources. Geophys. Res. Lett. 36, L20402.

Wahr, J., Molenaar, M., Bryan, F., 1998. Time variability of the Earth' s gravity field: hydrological and oceanic effects and their possible detection using GRACE. J. Geophys. Res. 103 (B12), 30,205–30,229.

Wang, S.L., Li, Z.F., Liu, J.S., Liang, Z.X., 1990. Study on the tritium (T) isotopes in the surface and ground waters on eastern Qinghai–Tibet Plateau. Environ. Sci. 11 (1), 24–27 (in Chinese).

Wang, H., Xiang, L., Jia, L., Jiang, L., Wang, Z., Hu, B., Gao, P., 2012. Load Love numbers and Green's functions for elastic Earth models PREM, iasp91, ak135, and modified models with refined crustal structure from Crust 2.0. Comput. Geosci. 49, 190–199.

Yao, T.D., Thompson, L., Yang, W., Yu, W.S., Gao, Y., Guo, X.J., Yang, X.X., Duan, K.Q., Zhao, H.B., Xu, B.Q., Pu, J.C., Lu, A.X., Xiang, Y., Kattel, D.B., Joswiak, D., 2012. Different glacier status with atmospheric circulations in Tibetan Plateau and surroundings. Nat. Clim. Change 2, 663–667.

Yi, S., Sun, W.K., 2014. Evaluation of glacier changes in high-mountain Asia based on 10 year GRACE RL05 models. J. Geophys. Res. 119, 2504–2517.

Zhang, G.Q., Xie, H.J., Kang, S.C., Yi, D.H., Ackley, S.F., 2011. Monitoring lake level changes on the Tibetan Plateau using ICESat altimetry data (2003–2009). Remote Sens. Environ. 115 (7), 1733–1742.

Zhang, G.Q., Yao, T.D., Xie, H.J., Kang, S.C., Lei, Y.B., 2013. Increased mass over the Tibetan Plateau: from lakes or glaciers? Geophys. Res. Lett. 40 (10), 2125–2130.

Zhong, M., Duan, J.B., Xu, H.Z., Peng, P., Yan, H.M., Zhu, Y.Z., 2009. Trend of China land water storage redistribution at medi- and large-spatial scales in recent five years by satellite gravity observations. Chin. Sci. Bull. 54 (5), 816–821.

Zhou, S.Q., Kang, S.C., Chen, F., Joswiak, D.R., 2013. Water balance observations reveal significant subsurface water seepage from Lake Nam Co, South-central Tibetan Plateau. J. Hydrol. 491, 89–99.